JACS
JOURNAL OF THE AMERICAN CHEMICAL SOCIETY

Editors' Choice
Open Access

pubs.acs.org/JACS

Article

A Flexible Phosphonate Metal–Organic Framework for Enhanced Cooperative Ammonia Capture

Dukula De Alwis Jayasinghe, Yinlin Chen, Jiangnan Li, Justyna M. Rogacka, Meredydd Kippax-Jones, Wanpeng Lu, Sergei Sapchenko, Jinyue Yang, Sarayute Chansai, Tianze Zhou, Lixia Guo, Yujie Ma, Longzhang Dong, Daniil Polyukhov, Lutong Shan, Yu Han, Danielle Crawshaw, Xiangdi Zeng, Zhaodong Zhu, Lewis Hughes, Mark D. Frogley, Pascal Manuel, Svemir Rudić, Yongqiang Cheng, Christopher Hardacre, Martin Schröder,* and Sihai Yang*

Cite This: J. Am. Chem. Soc. 2024, 146, 32040–32048

Read Online

ACCESS | Metrics & More | Article Recommendations | Supporting Information

ABSTRACT: Ammonia (NH_3) production in 2023 reached 150 million tons and is associated with potential concomitant production of up to 500 million tons of CO_2 each year. Efforts to produce green NH_3 are compromised since it is difficult to separate using conventional condensation chillers, but in situ separation with minimal cooling is challenging. While metal–organic framework materials offer some potential, they are often unstable and decompose in the presence of caustic and corrosive NH_3. Here, we address these challenges by developing a pore-expansion strategy utilizing the flexible phosphonate framework, STA-12(Ni), which shows exceptional stability and capture of NH_3 at ppm levels at elevated temperatures (100–220 °C) even under humid conditions. A remarkable NH_3 uptake of 4.76 mmol g^{-1} at 100 μbar (equivalent to 100 ppm) is observed, and in situ neutron powder diffraction, inelastic neutron scattering, and infrared microspectroscopy, coupled with modeling, reveal a pore expansion from triclinic to a rhombohedral structure on cooperative binding of NH_3 to unsaturated Ni(II) sites and phosphonate groups. STA-12(Ni) can be readily engineered into pellets or monoliths without losing adsorption capacity, underscoring its practical potential.

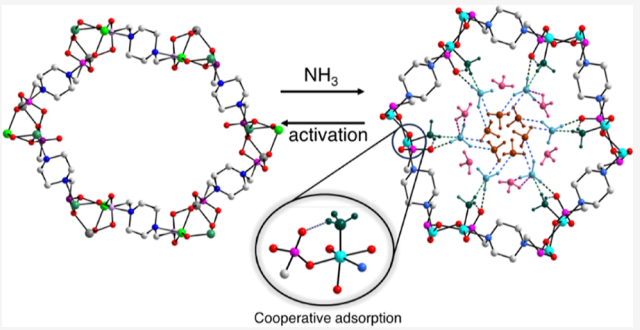

INTRODUCTION

Global NH_3 production, crucial for fertilizer and pharmaceutical production and as a hydrogen carrier, is expected to rise due to ever-increasing demand.[1−4] The Haber–Bosch process operates above 400 °C and at 150 bar and is linked to condensation chillers operating at −25 °C and 140 bar to recycle unreacted N_2 and H_2.[5] It is estimated that 1.87 tons of CO_2 are emitted per ton of NH_3 produced, accounting for 1.4–1.8% of global CO_2 emissions annually.[3] Efforts to decarbonize NH_3 production have led to the development of second-generation ruthenium catalysts that operate at 300–400 °C at lower pressures[6,7] and of greener routes using photo-[8,9] and electrocatalysts.[10] However, the separation of NH_3 via condensation is challenging as NH_3 is produced at low concentrations.[11,12] Successful capture and separation of NH_3 at low concentrations can potentially reduce capital costs by at least 5-fold.[13,14] Separation beds using metal halides such as $MgCl_2$ have been suggested as replacements for chillers as they exhibit high NH_3 uptake at low NH_3 partial pressures (0.002–0.1 bar) and show high-temperature operability.[15] However, they require high energy regeneration and often decompose after a few cycles with decreased NH_3 uptake efficiency.[16]

Metal–organic framework (MOF) materials have emerged as tunable sorbents due to their high NH_3 uptake capacities.[4,17−25] However, sorbents that combine high adsorption and capture efficacy at low pressures, coupled to stability against corrosive and caustic NH_3 under relevant conditions, such as high temperature and humidity, remain elusive.[26] To date, sorbents that satisfy the stringent requirements for effective and reliable NH_3 management in industrial settings remain limited. Herein, we establish a pathway to engineer a robust sorbent for NH_3 capture using a novel pore-expansion strategy that drives uptake by an increase in the entropy on substrate adsorption (i.e., a positive $\Delta S_{ads}^{\ddagger}$). The chemical stability of MOFs relies on the choice of metal ions and appropriate linkers, utilizing the enthalpy ($\Delta H_{ads}^{\ddagger}$) of metal–ligand binding to drive substrate uptake and avoid host

Received: September 7, 2024
Revised: October 17, 2024
Accepted: October 18, 2024
Published: November 8, 2024

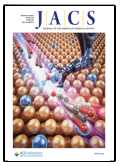

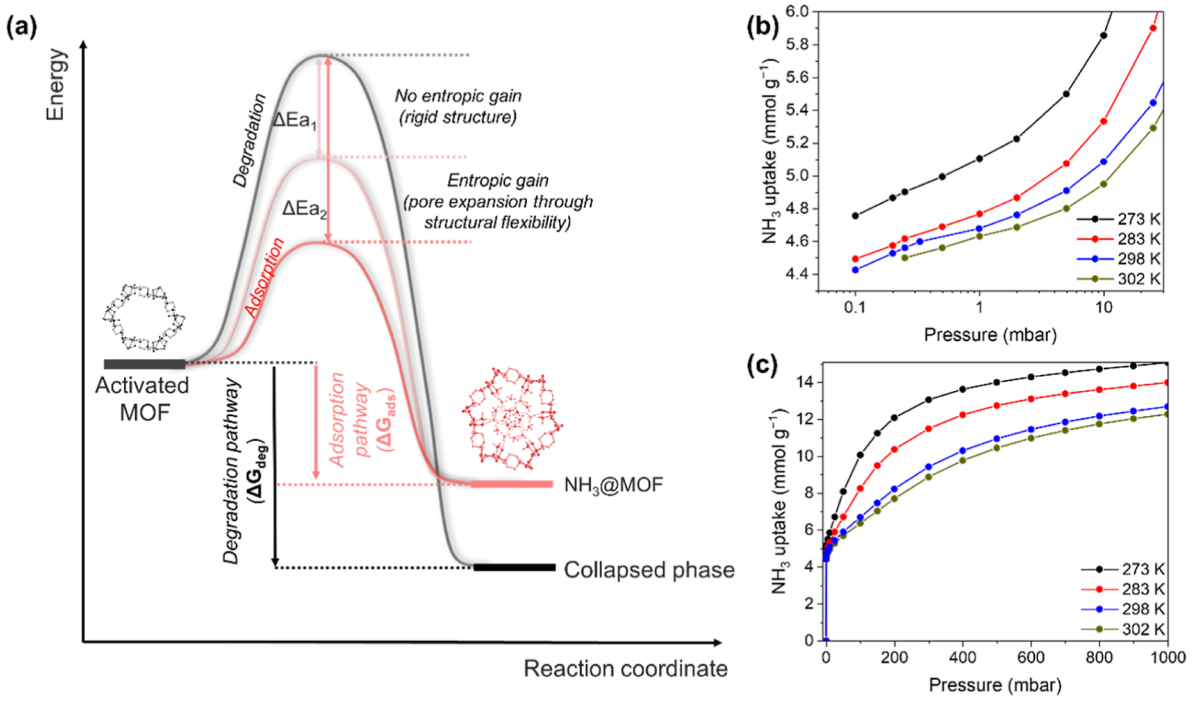

Figure 1. (a) Energy profile diagram for STA-12(Ni) depicting adsorption control using a pore-expansion strategy to favor adsorption over structural degradation (and desorption). Entropic gain facilitates adsorption by reducing the kinetic barrier (ΔEa_2) relative to the barrier for degradation. The activation energy barrier (ΔEa_1) between the adsorption and degradation pathways is smaller, increasing the likelihood of adsorption with structural collapse. (b,c) View of the low-pressure and overall NH_3 uptake of $[Ni_2(L)]$ between 273 and 302 K.

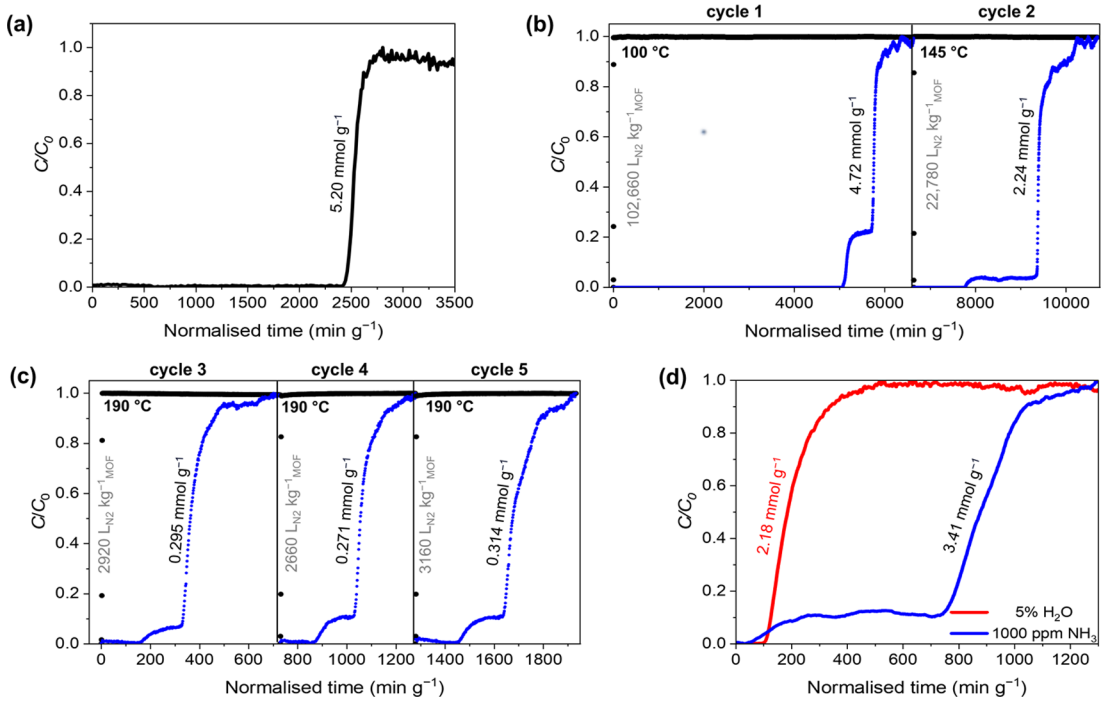

Figure 2. (a) Breakthrough of dry NH_3 through STA-12(Ni) using a 50 mL flow of 1000 ppm of NH_3 diluted in He at 298 K. Dry NH_3 breakthrough cycling experiments under a flow of 20 mL of 1000 ppm of NH_3 diluted in N_2 with STA-12(Ni) at (b) 100 and 145 °C (cycle 1 and 2) and (c) 190 °C (cycles 3−5). The N_2 working capacity in each cycle is shown in gray. (d) NH_3 and H_2O breakthrough at 150 °C through STA-12(Ni) under a flow of Ar containing 1000 ppm of NH_3 (blue) and 5% H_2O (100 mL/min).

degradation. On substrate uptake, there tends to be a net decrease in entropy (i.e., a negative $\Delta S^{\ddagger}_{ads}$) since polar gaseous adsorbates such as NH_3 become typically more ordered on adsorption within pores. Our strategy is based around the use of a flexible MOF to give an entropic drive for substrate adsorption through pore expansion, especially at low substrate partial pressure (Figure 1a), thus pivoting the system toward adsorption rather than structural degradation as is typically observed with NH_3 uptake in MOFs.[4,26]

https://doi.org/10.1021/jacs.4c12430
J. Am. Chem. Soc. 2024, 146, 32040−32048

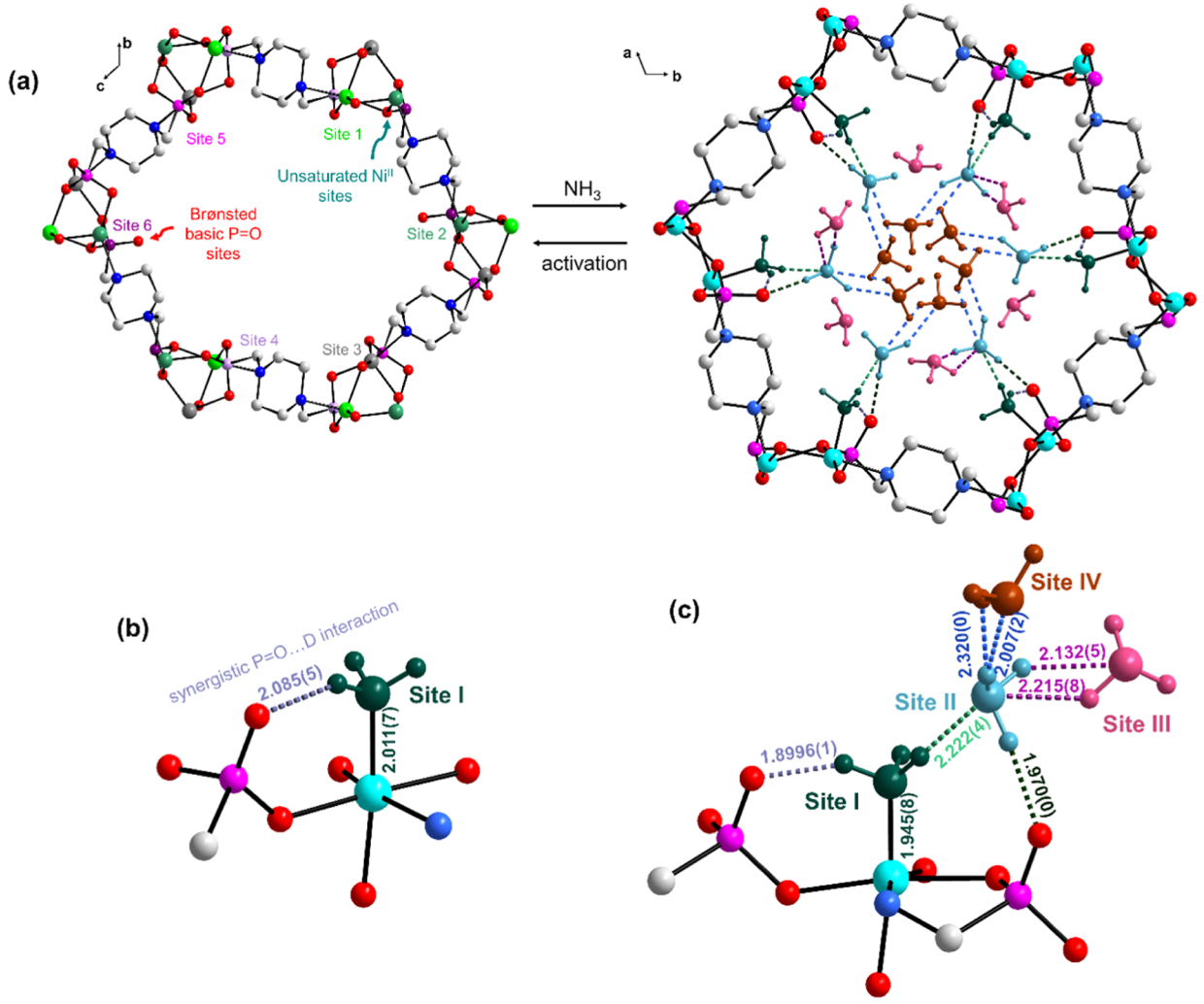

Figure 3. (a) View of structural transformation of STA-12(Ni) from triclinic (left) to rhombohedral (right) symmetry induced on NH_3 uptake, showing framework sites 1−6. View of binding sites in STA-12(Ni) of (b) low-loaded (0.95 ND_3/Ni) and (c) high-loaded (1.82 ND_3/Ni) [$Ni_2(L)$] showing sites I−IV for NH_3 positions. The Ni^{II}, N(ligand), C, O, and P atoms are shown in light blue, sea blue, white, red, and purple, respectively. ND_3 binding sites I to IV are highlighted in dark green, bright blue, cream pink, and maroon, respectively. The synergistic interactions between Brønsted basic P═O groups and Ni-bound chemisorbed NH_3 are also indicated.

RESULTS AND DISCUSSION

STA-12(Ni) is a phosphonate-based flexible MOF containing Ni(II) sites bridged by *N*,*N*′-piperazine-bis-(methylenephosphonate) linkers (L^{4-}).[27,28] Synthesis in water affords the fully hydrated rhombohedral framework, $[Ni_2(L)(H_2O)_2]\cdot 6H_2O$, which can be dehydrated (activated) by heating at 100 °C under a dynamic vacuum of 4×10^{-3} mbar for 6−8 h to constant weight to give the partially hydrated form of STA-12(Ni), $[Ni_2(L)(H_2O)_2]$, with H_2O bound to Ni(II). Heating at 170 °C under a dynamic vacuum of 4×10^{-5} mbar for 6 h affords a fully dehydrated (activated) form STA-12(Ni)$_{act}$, $[Ni_2(L)]$, incorporating a narrower triclinic framework.

Upon exposure to NH_3, STA-12(Ni)$_{act}$ undergoes a transformation to a rhombohedral structure, which induces a distinct stepped isotherm demonstrating a record-high NH_3 uptake of 4.76 mmol g^{-1} at an ultra-low pressure of 100 μbar (equivalent to 100 ppm) (Figure 1b,c). This is driven by NH_3 coordination to the Ni(II) sites to give an overall uptake of 15.0 mmol g^{-1} at 1 bar, 273 K (Figure 1c), corresponding to a high storage density of 0.34 g cm^{-3}. STA-12(Ni) can maintain its structural integrity through at least 90 adsorption−desorption cycles and remains stable after being immersed in an 18 M NH_3 solution for 30 h and boiling in the same solution for 2 h at 100 °C (Figure S1). This performance is underpinned by synergy between the Brønsted basic phosphonate moiety of the framework and the vacant metal site at Ni(II) that facilitates the binding of NH_3 to Ni(II) coupled to hydrogen bonding between NH_3 and P═O groups. This drives the packing of NH_3 close to that of solid NH_3 at 195 K,[29] as confirmed by neutron powder diffraction (NPD) and inelastic neutron scattering (INS) (see below).

STA-12(Ni)$_{act}$ undergoes a pore expansion on uptake of NH_3 leading to a net increase in entropy of ΔS = +79 J K^{-1} mol^{-1} on going from 4.5 to 7.0 mmol g^{-1} surface coverage (Figure S2). Thus, adsorption is favored over framework degradation and is supported by the enthalpic stability gained through Ni(II)−NH_3 bonding. The analogue STA-12(Mn), despite possessing the same structure, exhibits reduced stability toward NH_3 due to the kinetic lability of Mn(II) compared with Ni(II) (Figures S3 and S4). The rigid, isostructural STA-16(Ni) material, incorporating the extended linker *N*,*N*′-4,4′-

https://doi.org/10.1021/jacs.4c12430
J. Am. Chem. Soc. 2024, 146, 32040−32048

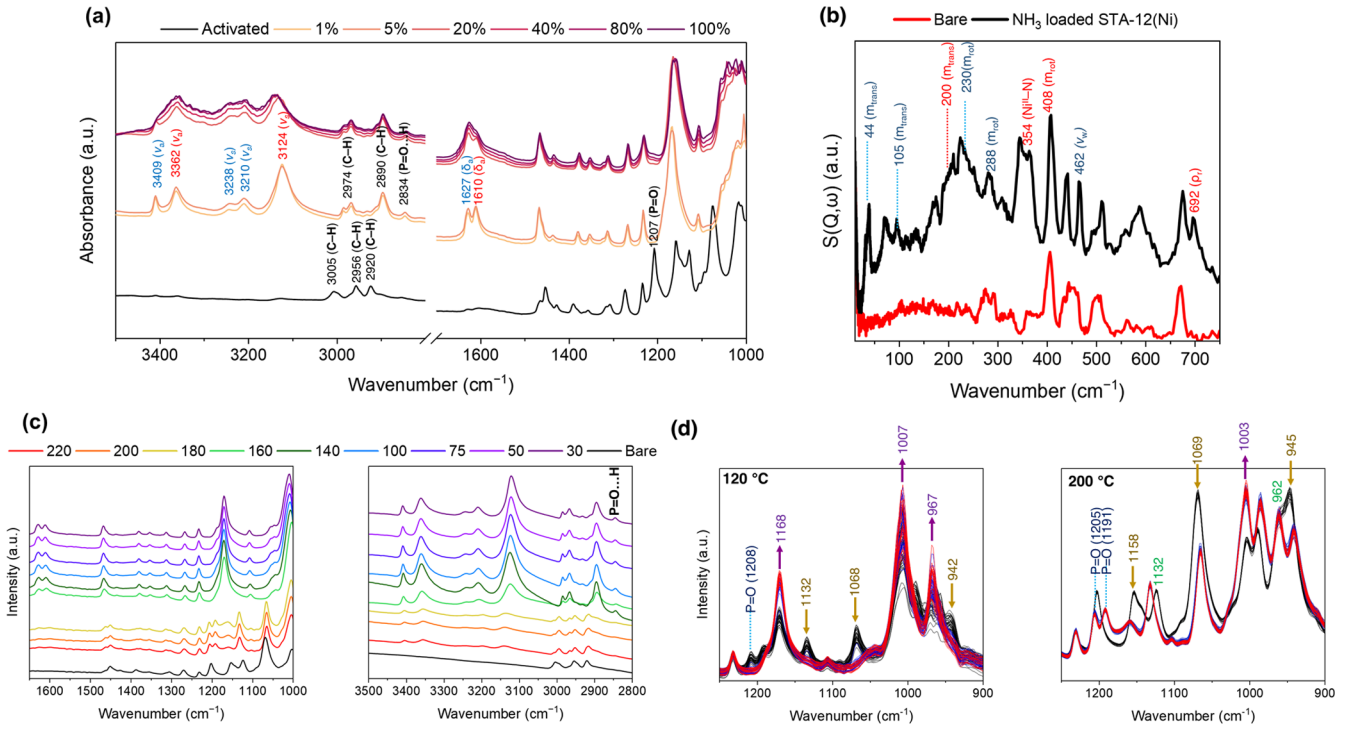

Figure 4. (a) In situ IR spectra of STA-12(Ni), $[Ni_2(L)]$, with increasing NH_3 loading and (b) experimental INS spectra of bare (red) and NH_3-loaded $[Ni_2(L)]$ (black). In both cases, vibrational and molecular motions associated with chemisorbed and physisorbed NH_3 are highlighted in red and dark blue, respectively. Bands associated with $[C-PO_3]^{2-}$ which decrease in intensity are marked in blue, with new bands indicated in purple. (c) IR spectra of $[Ni_2(L)]$ under a 100 mL flow of 1% NH_3 diluted in N_2 from 30 to 220 °C. (d) IR spectra obtained using rapid scans at 120 °C (left) and 200 °C (right) under flow; the color scheme indicates the time at which the spectra were obtained from the point of start of flow. In each case, the P═O group peaks are highlighted in blue. Bands associated with $[C-PO_3]^{2-}$ perturbations are also indicated; bands expected to decrease and increase are shown in brown and purple, respectively. The bands which did not undergo significant changes are highlighted in green.

bipiperidine-bis(methylenephosphonate),[30] demonstrates lower NH_3 uptake at low pressures (Figures S3 and S5) suggesting that the remarkable NH_3 uptake of STA-12(Ni) at 100 μbar is driven not only by entropic gain but also by the narrower pore structure.

Performance under Dynamic Conditions. The dynamic uptake of STA-12(Ni)$_{act}$ at 298 K under a flow of 1000 ppm of NH_3 in He was measured as 5.20 mmol g^{-1} (Figure 2a), consistent with the value obtained from the static uptake measurements and exemplifying its potential application in capturing NH_3 at low partial pressures. The purity of the gas emitted under flow through STA-12(Ni)$_{act}$ remains less than 6 ppm of NH_3 until full breakthrough is achieved. This level is lower than the dangerous (300 ppm) and short-term workplace exposure limits (50 ppm) for NH_3 as set by the National Institute for Occupational Safety and Health.[31]

To evaluate the applicability of STA-12(Ni)$_{act}$ for NH_3 capture at elevated temperatures, dynamic breakthrough experiments using a fixed-bed column of STA-12(Ni)$_{act}$ under a 1000 ppm flow of dry NH_3 diluted in N_2 were undertaken at 100, 145, and 190 °C (Figure 2b,c). The material could be readily recycled throughout these experiments. STA-12(Ni)$_{act}$ successfully captures and separates NH_3 under these harsh conditions and is comparable to alkaline metal halides.[32,33] In all cases, a high dynamic uptake corresponding to a distinctive two-step breakthrough was observed, attributed to competition between the different strengths of the NH_3 binding sites coupled with the structural dynamics of the framework. Crucially, STA-12(Ni)$_{act}$ generates N_2 in 99.998% purity at the outlet with working capacities of 102,660 and 22,780 L kg^{-1} at 100 and 145 °C, respectively. A high average dynamic uptake for NH_3 of 0.293 mmol g^{-1} is observed at 190 °C in the cycling experiment. In situ infrared (IR) microspectroscopy using pure NH_3 and NH_3 diluted to 1% and 10% in N_2, conditions replicating the Haber−Bosch process, confirms that the material is capable of adsorbing NH_3 from 25 to 275 °C (Figure S6). The capture of NH_3 under humid conditions is another challenging task, with most previous studies focusing on hydrophobic sorbents.[34,35] Remarkably, STA-12(Ni)$_{act}$ is also capable of capturing NH_3 effectively from a flow of 1000 ppm of NH_3 and 5% H_2O in Ar at 150 °C with a dynamic uptake of 3.41 mmol g^{-1} (Figure 2d). Heating NH_3-saturated STA-12(Ni) at 190 °C releases all of the captured NH_3. In an industrial setting, this would result in ca. 0.6 GJ ton$^{-1}_{NH_3}$ energy loss.[13] Under similar conditions, metal halides require heating to 300 °C for full regeneration, with a significant energy penalty of 3.4 GJ ton$^{-1}_{NH_3}$.

Visualization and Mechanism of Host−Guest Binding and Dynamics. To visualize the binding domains of NH_3 in STA-12(Ni), in situ NPD data for bare and ND_3-loaded STA-12(Ni) were collected with ND_3:Ni loadings of 0.96 (low loading) and 1.82 (high loading). Rietveld refinement of STA-12(Ni)$_{act}$, $[Ni_2(L)]$, confirmed three crystallographically distinct Ni^{II} sites (sites 1 to 3) and three $[C-PO_3]^{2-}$ sites (sites 4 to 6) (Figure 3a). Rietveld refinement of data for low loading confirmed the location of chemisorbed ND_3 molecules at site I (0.96 ND_3/Ni) with a Ni···ND_3 distance of 2.022 and a strong synergistic hydrogen bonding interaction P═O···D−N = 2.085 Å (Figure 3b). At high loading, three additional

https://doi.org/10.1021/jacs.4c12430
J. Am. Chem. Soc. 2024, 146, 32040−32048

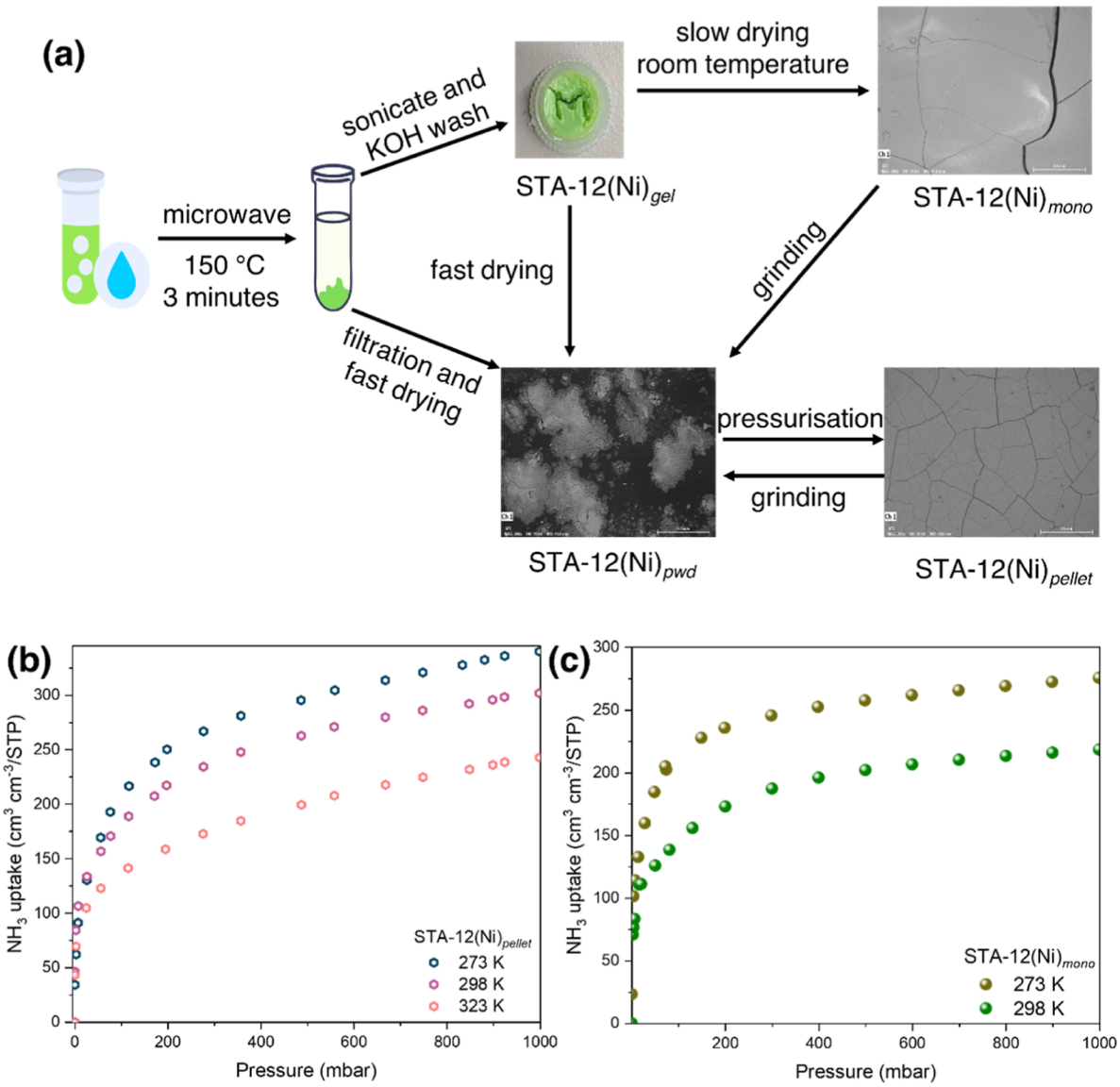

Figure 5. (a) Schematic of synthesis of powdered, gel, pelletized, and xerogel-derived monolithic forms of STA-12(Ni). Volumetric NH_3 uptakes of (b) fully activated $[Ni_2(L)]_{pellet}$ and (c) partially activated $[Ni_2(L)(H_2O)_2]_{mono}$.

binding sites for NH_3 (sites II–IV) were revealed (Figure 3c). At site I, with tighter substrate packing, the Ni···ND_3 and P═O···D–N distances decreased to 1.946 and 1.900 Å, respectively. Physisorbed ND_3 at site II with an occupancy of 0.67 ND_3/Ni revealed a further strong hydrogen bonding interaction with the P═O group and with other ND_3 molecules (P═O···D_3N = 1.972, ND···ND_3 = 2.222 Å). Site II further interacts with sites III and IV with ND_3:Ni occupancies of 0.181 and 0.046, respectively, and hydrogen bonding interactions (site III, ND···ND_3 = 2.1325; D_3N···DN = 2.216 Å, site IV, DN···D_3N = 2.036 Å). These are comparable to distances observed in solid NH_3 at 7 K (H_3N···HN_3 = 2.130 Å)[17] and confirm the presence of a combination of chemisorbed and physisorbed ND_3, amplified by strong synergistic interactions (Figure 3a) between the Brønsted basic phosphonate P═O groups and adsorbed NH_3 molecules. Furthermore, packing of NH_3 at a packing density of 0.74 g cm^{-3} at 273 K confirms its potential for NH_3 capture, storage, and transportation, particularly associated with the Haber–Bosch process.

The host–guest binding dynamics in this system were investigated further using a combination of in situ INS, density functional theory simulations, and in situ synchrotron IR microspectroscopy. Substantial changes in IR spectra upon loading of NH_3 into STA-12(Ni)$_{act}$ were observed due to the structural transition that occurs on NH_3 chemisorption (Figure 4a). Peaks associated with C–H stretching (3005–2920 cm^{-1}) convert to two bands centered at 2890 and 2970 cm^{-1} during NH_3 sorption, suggesting that the piperazine moieties become symmetrically equivalent. This is further confirmed through changes in the P–O vibrational region where bands at 1127, 1074, and 943 cm^{-1} decrease in intensity and peaks at 1158, 1011, and 965 cm^{-1} are generated. This suggests a significant distortion of the $[C\text{-}PO_3]^{2-}$ moieties, related to rotation of the $[C\text{-}PO_3]^{2-}$ tetrahedra at binding sites 4 and 5 during NH_3 chemisorption and the formation of symmetrically equivalent phosphonate tetrahedra. Bands corresponding to N–H stretches (3409–3124 cm^{-1}) and deformations (1627–1610 and 1184–1052 cm^{-1}) of physisorbed and chemisorbed NH_3 appear upon contact with NH_3. The rocking (ρ_r) and

https://doi.org/10.1021/jacs.4c12430
J. Am. Chem. Soc. 2024, 146, 32040–32048

stretching modes of Ni−NH_3 are observed at 683 and 354 cm^{-1}, respectively. IR bands associated with chemisorbed NH_3 shift and broaden with increasing NH_3 loading (Figure S7), consistent with the formation of hydrogen bonding between sites I and II. The presence of the symmetric N−H stretch of physisorbed NH_3 suggests the formation of NH_3 clusters facilitated by extensive hydrogen bonding interactions.[36,37] Interestingly, the band at 1207 cm^{-1} assigned to the P═O stretching mode weakens in intensity and red-shifts by ca. 18 cm^{-1} upon NH_3 loading due to weakening of the π bond of P═O via strong hydrogen bonding interactions. The appearance of the weak peak at 2834 cm^{-1} further suggests the formation of an intramolecular P−O···H interaction.[38]

The INS spectra (Figure 4b) reveal the molecular-level behavior of adsorbed NH_3. Rotational motion (m_{rot}) of chemisorbed and physisorbed NH_3 was observed at 408 and 288−230 cm^{-1}, and translational motion (m_{trans}) was observed at 200 and 105−53 cm^{-1}. This reflects the host-guest interactions of the NH_3 molecules with the framework. Compared to the INS spectra of solid NH_3,[17] bands associated with physisorbed NH_3 are blue-shifted and broadened, consistent with hydrogen bonding between NH_3 molecules and the framework. The increase in intensity of existing peaks associated with the framework dynamics upon NH_3 loading confirms responsiveness of the material toward NH_3.

IR spectroscopic measurements using a flow of 1% NH_3 diluted in N_2 (100 mL/min) between 25 and 220 °C confirmed the presence of both chemisorbed and physisorbed NH_3, with the intensities of the bands associated with the latter decreasing with an increase of temperature (Figure 4c). To investigate further the dynamics and adsorption mechanisms at higher temperatures, we undertook rapid IR measurements under flow at 120 and 200 °C. Significant differences were observed in the spectra at 200 °C compared with those at 120 °C. At 200 °C, instead of an increase, the band at 1158 cm^{-1} attributed to the $[C\text{-}PO_3]^{2-}$ moiety blue-shifts and decreases in intensity, while the band at 1125 cm^{-1} is blue-shifted to 1132 cm^{-1} but does not show a notable decrease (Figure 4d). The split and red shift of the band assigned to the P═O stretching mode is also clearly observed in these measurements; at 120 °C, the band initially at 1208 cm^{-1} slowly disappears, while a band at 1191 cm^{-1} grows, which then overlaps with the intense band at 1168 cm^{-1}. At 200 °C, these bands are clearer (1205 and 1191 cm^{-1}) since the intensity of the band at 1158 cm^{-1} associated with the $[C\text{-}PO_3]^{2-}$ unit is less intense. The band at 2834 cm^{-1} assigned to the P−O···H interaction also appears under these conditions (Figure 4c), becoming sharper at lower temperature, further illustrating the interplay of the Brønsted basic P═O sites in facilitating strong hydrogen bonding with NH_3. This indicates that adsorbed NH_3 is strongly immobilized with limited motion, consistent with INS data. These observations also suggest at elevated temperatures that only the accessible $[C\text{-}PO_3]^{2-}$ units rotate, and an intermediate between triclinic and rhombohedral symmetry exists upon NH_3 adsorption, possibly linked to partial coordination to Ni(II) sites within the structure. This also confirms that the driving force for NH_3 capture at high temperatures is linked to the associated increase in the entropy during adsorption. Computational modeling of the NH_3 isotherms further supports this hypothesis (Figure S8), which confirms a higher uptake for the rhombohedral framework with more accessible Ni(II) sites at lower pressure than the triclinic structure.

Scalable Material Synthesis and Engineering. We have also developed a microwave synthesis for STA-12(Ni) to give the material in greater than 75% yield (based on linker) in 3 min, a striking improvement over the published method (Figure S9).[27,28] It can also be prepared under reflux at 160 °C for 6 h (Figure S9), suggesting a route to a cost-effective scale-up of this material.[39]

Evaluation of sorbents is often based on their powdered forms and theoretical crystallographic framework densities. However, these theoretical values significantly differ from the practical densities. For example, the tapped density of STA-12(Ni) in powdered form, STA-12(Ni)$_{pwd}$, is ca. 0.057 g cm^{-3} (Figure S10), nearly 26 times less than its crystallographic density. Addressing this discrepancy, the compression of MOF powders into pellets to enhance packing efficiency and volumetric gas storage density is attractive, but this can potentially lead to mechanical collapse of the material resulting in lower uptakes.[40,41] Recent work has also highlighted monolithic forms of MOFs which can avoid such mechanical collapse.[42−44] We assessed the practicality of STA-12(Ni)$_{act}$ for sorption by processing it into pellets under 3 tonnes pressure (Figure 5a). STA-12(Ni)$_{pellet}$ shows a density of 1.14 g cm^{-3} with an overall gravimetric uptake at 1 bar for NH_3 only slightly reduced by 0.2 mmol g^{-1} compared to its powder form STA-12(Ni)$_{pwd}$ at 323 K. This represents only a 2% reduction in capacity (Figure S11). However, STA-12(Ni)$_{pellet}$ shows a volumetric NH_3 uptake of 289 cm^3 cm^{-3}/STP at 1 bar, 298 K (Figure 5b). This is significantly higher than the volumetric uptake of 15.3 cm^3 cm^{-3}/STP under the same conditions for fully activated STA-12(Ni)$_{pwd}$. This confirms the efficacy of pelletization for improved volumetric uptake capacities without compromising gravimetric uptake.

A xerogel-based monolithic form of STA-12(Ni) was prepared using a base-induced gelation method followed by slow-drying at room temperature (Figures 5a and S12−S19). Interestingly, the moldability of precursor STA-12(Ni)$_{gel}$ before drying offers flexibility in shaping the material to fit specific storage containers, presenting a potential higher packing efficiency than both pellet and powder forms. Drying of the gel form of STA-12(Ni)$_{gel}$ afforded the first example of monolithic phosphonate-based MOF STA-12(Ni)$_{mono}$ incorporating $[Ni_2(L)(H_2O)_2]$ with H_2O still bound to Ni(II). The fully dehydrated, activated form of the monolith could be prepared but collapses in air and in the presence of NH_3 presumably due to the bulk material undergoing structural transformation on coordination of NH_3 to Ni(II). A stable monolithic form could be generated by heating the sol−gel form at 100 °C under a dynamic vacuum of 4×10^{-3} mbar for 6−8 h to constant weight such that only physisorbed H_2O in the pore is removed, to yield STA-12(Ni)$_{mono}$, $[Ni_2(L)(H_2O)_2]$. STA-12(Ni)$_{mono}$ shows a density of 1.25 g cm^{-3} (Figure 5c) with a volumetric NH_3 uptake of 202 cm^3 cm^{-3}/STP at 1 bar, 298 K. We thus sought to compare the partially hydrated form of STA-12(Ni)$_{pwd}$ with all physisorbed H_2O molecules removed but with coordinated water still present within STA-12(Ni)$_{mono}$. At low pressure (<5 mbar NH_3), partially hydrated STA-12(Ni)$_{pwd}$ and STA-12(Ni)$_{mono}$ changed color to blue green suggesting NH_3 coordination to Ni(II) sites within the sample. STA-12(Ni)$_{mono}$ shows an NH_3 uptake of 202 cm^3 cm^{-3}/STP at 1 bar, 298 K (as described above), and partially hydrated STA-12(Ni)$_{pwd}$ has a tapped density of 0.063 g cm^{-3} and a much lower volumetric NH_3 uptake of 12.4 cm^3 cm^{-3}/STP confirming that monolith

https://doi.org/10.1021/jacs.4c12430
J. Am. Chem. Soc. 2024, 146, 32040−32048

formation affords a significant 16-fold improvement in NH_3 uptake. The NH_3-loaded materials can be fully rehydrated by washing with water. This is particularly useful in NH_3 capture during wastewater treatments, and this exchange of NH_3 under flow conditions was confirmed further using in situ synchrotron IR spectroscopy (Figure S20).

CONCLUSIONS

We confirm the use of STA-12(Ni) as a sorbent that meets the criteria for practical NH_3 capture and storage by demonstrating adaptability and stability under appropriate conditions. STA-12(Ni)$_{act}$ efficiently captures NH_3 at low concentrations and maintains efficacy across a wide temperature range (25−220 °C), marking a significant advance over existing sorbents. Its resilience, evidenced by sustained structural integrity even after rigorous NH_3 cycling and exposure to harsh environments including pure NH_3, is attributed to the increase in entropy due to structural change on substrate uptake, and the cooperative interaction between vacant metal sites and Brønsted basic phosphonate P═O groups to enhance binding and hydrogen bonding of trapped NH_3. The excellent performance of STA-12(Ni), particularly in pellet and monolithic forms, underscores its potential as a scalable and efficient solution for industrial NH_3 management challenges.

ASSOCIATED CONTENT

Supporting Information

The Supporting Information is available free of charge at https://pubs.acs.org/doi/10.1021/jacs.4c12430.

Synthesis, characterization, and analysis of NH_3-loaded materials and neutron diffraction, INS, modeling, and synchrotron IR microspectroscopy data (PDF)

AUTHOR INFORMATION

Corresponding Authors

Martin Schröder − *Department of Chemistry, The University of Manchester, Manchester M13 9PL, U.K.;* orcid.org/0000-0001-6992-0700; Email: m.schroder@manchester.ac.uk

Sihai Yang − *Department of Chemistry, The University of Manchester, Manchester M13 9PL, U.K.; College of Chemistry and Molecular Engineering, Beijing National Laboratory for Molecular Sciences, Peking University, Beijing 100871, China;* orcid.org/0000-0002-1111-9272; Email: sihai.yang@pku.edu.cn

Authors

Dukula De Alwis Jayasinghe − *Department of Chemistry, The University of Manchester, Manchester M13 9PL, U.K.*

Yinlin Chen − *Department of Chemistry, The University of Manchester, Manchester M13 9PL, U.K.*

Jiangnan Li − *College of Chemistry and Molecular Engineering, Beijing National Laboratory for Molecular Sciences, Peking University, Beijing 100871, China*

Justyna M. Rogacka − *Department of Chemistry, The University of Manchester, Manchester M13 9PL, U.K.; Department of Micro, Nano and Bioprocess Engineering, Faculty of Chemistry Wroclaw University of Science and Technology, Wroclaw 50-370, Poland*

Meredydd Kippax−Jones − *Department of Chemistry, The University of Manchester, Manchester M13 9PL, U.K.; Diamond Light Source, Oxfordshire OX11 0DE, U.K.*

Wanpeng Lu − *Department of Chemistry, The University of Manchester, Manchester M13 9PL, U.K.*

Sergei Sapchenko − *Department of Chemistry, The University of Manchester, Manchester M13 9PL, U.K.*

Jinyue Yang − *Department of Chemistry, The University of Manchester, Manchester M13 9PL, U.K.*

Sarayute Chansai − *Department of Chemical Engineering, The University of Manchester, Manchester M13 9PL, U.K.*

Tianze Zhou − *Department of Chemistry, The University of Manchester, Manchester M13 9PL, U.K.*

Lixia Guo − *College of Chemistry and Molecular Engineering, Beijing National Laboratory for Molecular Sciences, Peking University, Beijing 100871, China*

Yujie Ma − *Department of Chemistry, The University of Manchester, Manchester M13 9PL, U.K.;* orcid.org/0000-0002-6671-4650

Longzhang Dong − *Department of Chemistry, The University of Manchester, Manchester M13 9PL, U.K.*

Daniil Polyukhov − *Department of Chemistry, The University of Manchester, Manchester M13 9PL, U.K.*

Lutong Shan − *Department of Chemistry, The University of Manchester, Manchester M13 9PL, U.K.*

Yu Han − *Department of Chemistry, The University of Manchester, Manchester M13 9PL, U.K.*

Danielle Crawshaw − *Department of Chemistry, The University of Manchester, Manchester M13 9PL, U.K.*

Xiangdi Zeng − *Department of Chemistry, The University of Manchester, Manchester M13 9PL, U.K.*

Zhaodong Zhu − *Department of Chemistry, The University of Manchester, Manchester M13 9PL, U.K.*

Lewis Hughes − *Department of Earth and Environmental Sciences, The University of Manchester, Manchester M13 9PL, U.K.*

Mark D. Frogley − *Diamond Light Source, Oxfordshire OX11 0DE, U.K.*

Pascal Manuel − *ISIS Neutron and Muon Facility, Rutherford Appleton Laboratory, Chilton OX11 0QX, U.K.*

Svemir Rudić − *ISIS Neutron and Muon Facility, Rutherford Appleton Laboratory, Chilton OX11 0QX, U.K.;* orcid.org/0000-0003-3023-8565

Yongqiang Cheng − *Neutron Scattering Division, Neutron Sciences Directorate, Oak Ridge National Laboratory, Oak Ridge, Tennessee 37831, United States;* orcid.org/0000-0002-3263-4812

Christopher Hardacre − *Department of Chemical Engineering, The University of Manchester, Manchester M13 9PL, U.K.;* orcid.org/0000-0001-7256-6765

Complete contact information is available at: https://pubs.acs.org/10.1021/jacs.4c12430

Notes

The authors declare no competing financial interest.

ACKNOWLEDGMENTS

We thank the EPSRC (EP/I011870 and EP/V056409), the University of Manchester, National Science Foundation of China, Peking University, and BNLMS for funding. This project has received funding from the European Research Council (ERC) under the European Union's Horizon 2020 research and innovation programme (grant agreement no. 742401, NANOCHEM, and grant agreement no. 715502, EvoluTEM). We are grateful to the Diamond Light Source and

STFC/ISIS Facility for the access to beamtimes B22 and TOSCA/WISH, respectively. L.G., J.Y., J.M., L.S., and Y.H. thank the China Scholarship Council (CSC) for funding. J.R. is supported by the Polish National Agency for Academic Exchange (decision no. BPN/BEK/2022/1/00053/DEC/1). This research used computing resources made available through the VirtuES and the ICE-MAN projects, funded by Laboratory Directed Research and Development program and Compute and Data Environment for Science (CADES) at ORNL, as well as resources of the National Energy Research Scientific Computing Centre (NERSC), a U.S. Department of Energy Office of Science User Facility located at Lawrence Berkeley National Laboratory, operated under contract no. DE-AC02-05CH11231 using NERSC award ERCAP0024340. Molecular simulations have been carried out in Wroclaw Center for Networking and Supercomputing (http://www.wcss.pl).

REFERENCES

(1) *Mineral Commodity Summaries—Nitrogen (Fixed)—Ammonia*; U.S. Geological Survey, 2024. https://pubs.usgs.gov/periodicals/mcs2024/mcs2024-nitrogen.pdf (accessed 2024−09−06).

(2) Ammonia: Zero-carbon Fertiliser *Fuel and Energy Store*. The Royal Society, 2020. https://royalsociety.org/news-resources/projects/low-carbon-energy-programme/green-ammonia/(accessed 2024−09−06).

(3) Wang, Y.; Meyer, T. J. A Route to Renewable Energy Triggered by the Haber-Bosch Process. *Chem.* **2019**, *5*, 496−497.

(4) Han, X.; Yang, S.; Schröder, M. Metal−organic Framework Materials for Production and Distribution of Ammonia. *J. Am. Chem. Soc.* **2023**, *145*, 1998−2012.

(5) Walter, M. D. Ammonia Formation Revisited. *Nat. Chem.* **2022**, *14*, 12−13.

(6) Wang, Q.; Pan, J.; Guo, J.; Hansen, H. A.; Xie, H.; Jiang, L.; Hua, L.; Li, H.; Guan, Y.; Wang, P.; Gao, W.; Liu, L.; Cao, H.; Xiong, Z.; Vegge, T.; Chen, P. Ternary Ruthenium Complex Hydrides for Ammonia Synthesis via the Associative Mechanism. *Nat. Catal.* **2021**, *4*, 959−967.

(7) Wu, S.; Peng, Y.; Chen, T.-Y.; Mo, J.; Large, A.; McPherson, I.; Chou, H.-L.; Wilkinson, I.; Venturini, F.; Grinter, D.; Ferrer Escorihuela, P.; Held, G.; Tsang, S. C. E. Removal of Hydrogen Poisoning by Electrostatically Polar MgO Support for Low-ressure NH_3 Synthesis at a High Rate over the Ru Catalyst. *ACS Catal.* **2020**, *10*, 5614−5622.

(8) Han, Q.; Jiao, H.; Xiong, L.; Tang, J. Progress and Challenges in Photocatalytic Ammonia Synthesis. *Mater. Adv.* **2021**, *2*, 564−581.

(9) Kim, S.; Park, Y.; Kim, J.; Pabst, T. P.; Chirik, P. J. Ammonia Synthesis by Photocatalytic Hydrogenation of a N_2-Derived Molybdenum Nitride. *Nat. Synth.* **2022**, *1*, 297−303.

(10) Du, H.-L.; Chatti, M.; Hodgetts, R. Y.; Cherepanov, P. V.; Nguyen, C. K.; Matuszek, K.; MacFarlane, D. R.; Simonov, A. N. Electroreduction of Nitrogen with Almost 100% Current-to-Ammonia Efficiency. *Nature* **2022**, *609*, 722−727.

(11) Torrente-Murciano, L.; Smith, C. Process Challenges of Green Ammonia Production. *Nat. Synth.* **2023**, *2*, 587−588.

(12) Wang, M.; Khan, M. A.; Mohsin, I.; Wicks, J.; Ip, A. H.; Sumon, K. Z.; Dinh, C.-T.; Sargent, E. H.; Gates, I. D.; Kibria, M. G. Can Sustainable Ammonia Synthesis Pathways Compete with Fossil-Fuel Based Haber−Bosch Processes? *Energy Environ. Sci.* **2021**, *14*, 2535−2548.

(13) Smith, C.; Hill, A. K.; Torrente-Murciano, L. Current and Future Role of Haber−Bosch Ammonia in a Carbon-Free Energy Landscape. *Energy Environ. Sci.* **2020**, *13*, 331−344.

(14) Smith, C.; McCormick, A. V.; Cussler, E. L. Optimizing the Conditions for Ammonia Production Using Absorption. *ACS Sustainable Chem. Eng.* **2019**, *7*, 4019−4029.

(15) Onuoha, C. E.; Kale, M. J.; Malmali, M.; Dauenhauer, P. J.; McCormick, A. V. Improving Absorbent-Enhanced Ammonia Separation for Efficient Small-Scale Ammonia Synthesis. *Ind. Eng. Chem. Res.* **2024**, *63*, 5608−5617.

(16) Cao, Z.; Akhtar, F. Porous Strontium Chloride Scaffolded by Graphene Networks as Ammonia Carriers. *Adv. Funct. Mater.* **2021**, *31*, 2008505.

(17) Ma, Y.; Lu, W.; Han, X.; Chen, Y.; da Silva, I.; Lee, D.; Sheveleva, A. M.; Wang, Z.; Li, J.; Li, W.; Fan, M.; Xu, S.; Tuna, F.; McInnes, E. J. L.; Cheng, Y.; Rudić, S.; Manuel, P.; Frogley, M. D.; Ramirez-Cuesta, A. J.; Schröder, M.; Yang, S. Direct Observation of Ammonia Storage in UiO-66 Incorporating Cu(II) Binding Sites. *J. Am. Chem. Soc.* **2022**, *144*, 8624−8632.

(18) Snyder, B. E. R.; Turkiewicz, A. B.; Furukawa, H.; Paley, M. V.; Velasquez, E. O.; Dods, M. N.; Long, J. R. A Ligand Insertion Mechanism for Cooperative NH_3 Capture in Metal−Organic Frameworks. *Nature* **2023**, *613*, 287−291.

(19) Marsh, C.; Han, X.; Li, J.; Lu, Z.; Argent, S. P.; da Silva, I.; Cheng, Y.; Daemen, L. L.; Ramirez-Cuesta, A. J.; Thompson, S. P.; Blake, A. J.; Yang, S.; Schröder, M. Exceptional Packing Density of Ammonia in a Dual-Functionalized Metal−Organic Framework. *J. Am. Chem. Soc.* **2021**, *143*, 6586−6592.

(20) Tan, K.; Ullah, S.; Pandey, H.; Cedeño-Morales, E. M.; Wang, H.; Wang, K.; Zhou, H.-C.; Li, J.; Thonhauser, T. Competitive Adsorption of NHCompetitive Adsorption of NH_3 and H_2O in Metal−Organic Framework Materials: MOF-74 and H_2O in Metal−Organic Framework Materials: MOF-74. *Chem. Mater.* **2022**, *34*, 7906−7915.

(21) Han, X.; Lu, W.; Chen, Y.; da Silva, I.; Li, J.; Lin, L.; Li, W.; Sheveleva, A. M.; Godfrey, H. G. W.; Lu, Z.; Tuna, F.; McInnes, E. J. L.; Cheng, Y.; Daemen, L. L.; Mpherson, L. J. M.; Teat, S. J.; Frogley, M. D.; Rudić, S.; Manuel, P.; Ramirez-Cuesta, A. J.; Yang, S.; Schröder, M. High Ammonia Adsorption in MFM-300 Materials: Dynamics and Charge Transfer in Host−Guest Binding. *J. Am. Chem. Soc.* **2021**, *143*, 3153−3161.

(22) Guo, L.; Hurd, J.; He, M.; Lu, W.; Li, J.; Crawshaw, D.; Fan, M.; Sapchenko, S.; Chen, Y.; Zeng, X.; Kippax-Jones, M.; Huang, W.; Zhu, Z.; Manuel, P.; Frogley, M. D.; Lee, D.; Schröder, M.; Yang, S. Efficient Capture and Storage of Ammonia in Robust Aluminium-Based Metal−Organic Frameworks. *Commun. Chem.* **2023**, *6*, 55.

(23) Kim, D. W.; Kang, D. W.; Kang, M.; Choi, D. S.; Yun, H.; Kim, S. Y.; Lee, S. M.; Lee, J.-H.; Hong, C. S. High Gravimetric and Volumetric Ammonia Capacities in Robust Metal−Organic Frameworks Prepared via Double Postsynthetic Modification. *J. Am. Chem. Soc.* **2022**, *144*, 9672−9683.

(24) Rieth, A. J.; Tulchinsky, Y.; Dincă, M. High and Reversible Ammonia Uptake in Mesoporous Azolate Metal−Organic Frameworks with Open Mn, Co, and Ni Sites. *J. Am. Chem. Soc.* **2016**, *138*, 9401−9404.

(25) Rieth, A. J.; Dincă, M. Controlled Gas Uptake in Metal−Organic Frameworks with Record Ammonia Sorption. *J. Am. Chem. Soc.* **2018**, *140*, 3461−3466.

(26) Rieth, A. J.; Wright, A. M.; Dincă, M. Kinetic Stability of Metal−Organic Frameworks for Corrosive and Coordinating Gas Capture. *Nat. Rev. Mater.* **2019**, *4*, 708−725.

(27) Miller, S. R.; Pearce, G. M.; Wright, P. A.; Bonino, F.; Chavan, S.; Bordiga, S.; Margiolaki, I.; Guillou, N.; Férey, G.; Bourrelly, S.; Llewellyn, P. L. Structural Transformations and Adsorption of Fuel-Related Gases of a Structurally Responsive Nickel Phosphonate Metal−Organic Framework, Ni-STA-12. *J. Am. Chem. Soc.* **2008**, *130*, 15967−15981.

(28) Wharmby, M. T.; Pearce, G. M.; Mowat, J. P. S.; Griffin, J. M.; Ashbrook, S. E.; Wright, P. A.; Schilling, L.-H.; Lieb, A.; Stock, N.; Chavan, S.; Bordiga, S.; Garcia, E.; Pirngruber, G. D.; Vreeke, M.; Gora, L. Synthesis and Crystal Chemistry of the STA-12 Family of Metal N,N′-Piperazinebis(methylenephosphonate)s and Applications of STA-12(Ni) in the Separation of Gases. *Microporous Mesoporous Mater.* **2012**, *157*, 3−17.

(29) Otto, J. W.; Porter, R. F.; Ruoff, A. L. Equation of State of Solid Ammonia (NH_3) to 56 GPa. *J. Phys. Chem. Solids* **1989**, *50*, 171−175.
(30) Wharmby, M. T.; Mowat, J. P. S.; Thompson, S. P.; Wright, P. A. Extending the Pore Size of Crystalline Metal Phosphonates toward the Mesoporous Regime by Isoreticular Synthesis. *J. Am. Chem. Soc.* **2011**, *133*, 1266−1269.
(31) Ammonia, The National Institute for Occupational Safety and Health (NIOSH), 2019. https://www.cdc.gov/niosh/topics/ammonia/default.html (accessed 2024-09-06).
(32) Liu, C. Y.; Aika, K.-i. Ammonia Absorption into Alkaline Earth Metal Halide Mixtures as an Ammonia Storage Material. *Ind. Eng. Chem. Res.* **2004**, *43*, 7484−7491.
(33) Malmali, M.; Le, G.; Hendrickson, J.; Prince, J.; McCormick, A. V.; Cussler, E. L. Better Absorbents for Ammonia Separation. *ACS Sustain. Chem. Eng.* **2018**, *6*, 6536−6546.
(34) Liu, Z.; Wang, X.; Liu, Y.; Li, L.; Li, S. Computational Screening of Metal−Organic Frameworks for Ammonia Capture from Humid Air. *Microporous Mesoporous Mater.* **2022**, *331*, 111659.
(35) Moghadam, P. Z.; Fairen-Jimenez, D.; Snurr, R. Q. Efficient Identification of Hydrophobic MOFs: Application in the Capture of Toxic Industrial Chemicals. *J. Mater. Chem. A* **2016**, *4*, 529−536.
(36) Malloum, A.; Fifen, J. J.; Conradie, J. Structures and Infrared Spectroscopy of Large Sized Protonated Ammonia Clusters. *J. Chem. Phys.* **2018**, *149*, 244301.
(37) Wang, B.; Hou, P.; Cai, Y.; Guo, Z.; Han, D.; Gao, Y.; Zhao, L. Understanding the Hydrogen-Bonded Clusters of Ammonia $(NH_3)n$ (n = 3−6):Insights from the Electronic Structure Theory. *ACS Omega* **2020**, *5*, 31724−31729.
(38) Thomas, L. C.; Chittenden, R. A. Infrared Absorption Bands Associated with the POH Group. *J. Opt. Soc. Am.* **1962**, *52*, 829.
(39) Severino, M. I.; Gkaniatsou, E.; Nouar, F.; Pinto, M. L.; Serre, C. MOFs Industrialization: A Complete Assessment of Production Costs. *Faraday Discuss.* **2021**, *231*, 326−341.
(40) Yeskendir, B.; Dacquin, J.-P.; Lorgouilloux, Y.; Courtois, C.; Royer, S.; Dhainaut, J. From Metal−Organic Framework Powders to Shaped Solids: Recent Developments and Challenges. *Mater. Adv.* **2021**, *2*, 7139−7186.
(41) Tian, T.; Velazquez-Garcia, J.; Bennett, T. D.; Fairen-Jimenez, D. Mechanically and Chemically Robust ZIF-8 Monoliths with High Volumetric Adsorption Capacity. *J. Mater. Chem. A* **2015**, *3*, 2999−3005.
(42) Peng, Y.; Krungleviciute, V.; Eryazici, I.; Hupp, J. T.; Farha, O. K.; Yildirim, T. Methane Storage in Metal−Organic Frameworks: Current Records, Surprise Findings, and Challenges. *J. Am. Chem. Soc.* **2013**, *135*, 11887−11894.
(43) Tian, T.; Zeng, Z.; Vulpe, D.; Casco, M. E.; Divitini, G.; Midgley, P. A.; Silvestre-Albero, J.; Tan, J.-C.; Moghadam, P. Z.; Fairen-Jimenez, D. A Sol−Gel Monolithic Metal−Organic Framework with Enhanced Methane Uptake. *Nat. Mater.* **2018**, *17*, 174−179.
(44) Qi, X.; Liu, K.; Chang, Z. Beyond powders: Monoliths on the basis of metal-organic frameworks (MOFs). *Chem. Eng. J.* **2022**, *441*, 135953.

https://doi.org/10.1021/jacs.4c12430
J. Am. Chem. Soc. 2024, 146, 32040−32048